


RESEARCH ARTICLE

A *Plasmodium* homolog of ER tubule-forming proteins is required for parasite virulence

Xiaoyu Shi¹ | Lei Hai¹ | Kavitha Govindasamy² | Jian Gao¹ | Isabelle Coppens³ | Junjie Hu⁴ | Qian Wang^{1,4} | Purnima Bhanot ²

¹Department of Immunology, School of Basic Medical Sciences, Tianjin Key Laboratory of Cellular and Molecular Immunology, Key Laboratory of Immune Microenvironment and Diseases of Educational Ministry of China, Tianjin Medical University, Tianjin, China

²Department of Microbiology, Biochemistry and Molecular Genetics, Rutgers New Jersey Medical School, Newark, NJ, USA

³Department of Molecular Microbiology and Immunology, The Johns Hopkins University Bloomberg School of Public Health, Baltimore, MD, USA

⁴National Laboratory of Biomacromolecules, Institute of Biophysics, Chinese Academy of Sciences, Beijing, China

Correspondence

Qian Wang, Department of Immunology, School of Basic Medical Sciences, Tianjin Medical University, Tianjin Key Laboratory of Cellular and Molecular Immunology, Key Laboratory of Immune Microenvironment and Diseases of Educational Ministry of China, Tianjin 300070, China; National Laboratory of Biomacromolecules, Institute of Biophysics, Chinese Academy of Sciences, Beijing 100101, China.

Email: wangq@tmu.edu.cn

Purnima Bhanot, Rutgers New Jersey Medical School, Department of Microbiology, Biochemistry and Molecular Genetics, Newark, NJ 07103, USA.

Email: bhanotpu@njms.rutgers.edu

Funding information

Tianjin Medical University, Grant/Award Number: 115004/000012 and 11601502/DW0114; The Science & Technology Development Fund of Tianjin Education Commission for Higher Education, Grant/Award Number: 2018KJ085 and 2016KJ0138; National Institutes of Health, Grant/Award Number: 5R01AI133633 and R21AI128052; National Key Research and Development Program, Grant/Award Number: 2016YFA0500201; Open project supported by the National Laboratory of Biomacromolecules: 2018kf05; National Natural Science Foundation of China, Grant/Award Number: 31630020 and 91854202

Abstract

Reticulon and REEP family of proteins stabilize the high curvature of endoplasmic reticulum (ER) tubules. *Plasmodium berghei* Yop1 (*PbYop1*) is a REEP5 homolog in *Plasmodium*. Here, we characterize its function using a gene-knockout (*Pbyop1Δ*). *Pbyop1Δ* asexual stage parasites display abnormal ER architecture and an enlarged digestive vacuole. The erythrocytic cycle of *Pbyop1Δ* parasites is severely attenuated and the incidence of experimental cerebral malaria is significantly decreased in *Pbyop1Δ*-infected mice. *Pbyop1Δ* sporozoites have reduced speed, are slower to invade host cells but give rise to equal numbers of infected HepG2 cells, as WT sporozoites. We propose that *PbYOP1*'s disruption may lead to defects in trafficking and secretion of a subset of proteins required for parasite development and invasion of erythrocytes. Furthermore, the maintenance of ER morphology in different parasite stages is likely to depend on different proteins.

KEYWORDS

DP1, endoplasmic reticulum, REEP, reticulon, YOP1

1 | INTRODUCTION

In eukaryotic cells, the endoplasmic reticulum (ER) is a continuous membrane system that is involved in protein translation, secretion, calcium

homeostasis, and lipid biosynthesis (Baumann and Walz, 2001). It makes membrane contacts with the plasma membrane, endosomes, and mitochondria, which enable it to play a pivotal role in inter-organellar communication (reviewed in Wu *et al.*, 2018). Its morphology, consisting

of subdomains of sheet structures and an interconnected network of tubules, is tightly associated with its physiological functions (Shibata *et al.*, 2006; Wang *et al.*, 2017). The relative ratio of these structural domains in the ER is modified in different cell types to fulfill specific functional requirements. For example, the ER of professional secretory cells, such as pancreatic cells, consist almost entirely of sheets while the ER of nonsecretory cells, such as neurons, have abundant tubular networks (Hu *et al.*, 2009; Westrate *et al.*, 2015). Just a handful of studies have examined ER morphology in protozoa (van Dooren *et al.*, 2005; Teixeira and Huston, 2008; Nishi *et al.*, 2008; Kaiser *et al.*, 2016) and none have studied its specification at a molecular level.

The malaria-causing protozoan, *Plasmodium* undergoes a complex life cycle in the mammalian host and the mosquito vector. It sequentially infects mammalian hepatocytes and erythrocytes, and undergoes a multistep developmental program within them. The resulting increase in parasite numbers causes pathology in the host and ensures transmission to the vector. During *Plasmodium*'s intraerythrocytic and intrahepatic development, its ER transforms from a primarily perinuclear structure without a distinctive morphological character in early stages, into a dense, interconnected network of tubules with aggregations throughout the cytoplasm as the parasite enlarges (van Dooren *et al.*, 2005; Kaiser *et al.*, 2016). In hepatic and erythrocytic merozoites, the ER is perinuclear with peripheral protrusions into the cytoplasm (Kaiser *et al.*, 2016). In sporozoites, parasite stages that are transmitted to humans via mosquito bite, *Plasmodium*'s ER is also perinuclear and extends into the cytoplasm but does not form a dense network (Kaiser *et al.*, 2016). How this dynamic ER morphology is specified and maintained through different developmental stages of the parasite is not understood.

Higher eukaryotes are known to use specific classes of integral membrane proteins to shape the ER. Tubules are generated and maintained through the action of Yop1p (nomenclature in yeast, termed DP1 or REEP5 in mammalian cells) and reticulon (RTN) family of proteins that induce high curvature in the membrane (Voeltz *et al.*, 2006; Anderson and Hetzer, 2008). The reticulon-homology domain of membrane-curving proteins consists of two hydrophobic regions that form transmembrane hairpins that occupy more space in the outer leaflet than the inner leaflet of the lipid bilayer, thus deforming membranes as a wedge insertion. A conserved amphipathic helix downstream of the second transmembrane domain can provide additional wedging (Brady *et al.*, 2015). To form a network, ER tubules are fused together in a GTP-dependent manner through the action of Sey1p proteins (nomenclature in yeast, termed atlastin/ATL GTPases in mammalian cells; Hu *et al.*, 2009; Orso *et al.*, 2009). Additional proteins, such as Lunapark (Lnp) also play a role in maintaining a balance of tubules and sheets (Chen *et al.*, 2012; Shemesh *et al.*, 2014; Chen *et al.*, 2015; Wang *et al.*, 2016; Wang *et al.*, 2018; Zhou *et al.*, 2019).

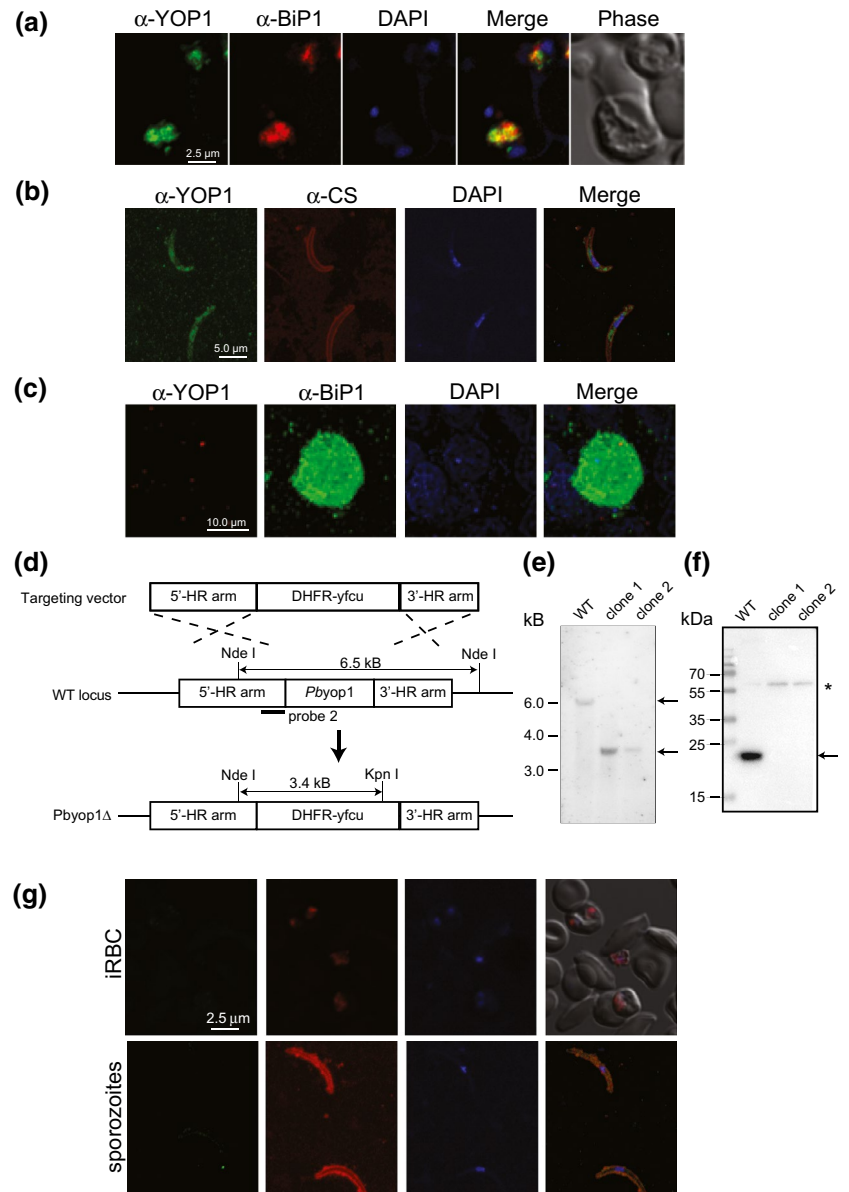
The physiological importance of maintaining ER morphology is underscored by serious defects observed in organisms, as varied as humans and plants, when ER-shaping proteins are disrupted. In humans, mutations in ER-shaping proteins RTN2, REEP1, and ATL1 are associated with a constellation of genetically-encoded neurological

defects, collectively termed Hereditary spastic paraplegias (HSPs; reviewed in Blackstone *et al.*, 2011, because they compromise axonal maintenance and function (Allison *et al.*, 2017; Yalcin *et al.*, 2017);). Lnp mutations cause a recessive neurodevelopmental syndrome (Breuss *et al.*, 2018). Forms of retinitis pigmentosa, a progressive form of blindness, are attributed to defects in secretion caused by mutations in REEP6, a human Yop1p homolog (Agrawal *et al.*, 2017; Veleri *et al.*, 2017). REEP5 is required for cardiac function (Yao *et al.*, 2018; Lee *et al.*, 2020). In plants, disruptions of ER-shaping proteins inhibit vesicular trafficking and cause developmental defects in the formation of root hairs (Galway *et al.*, 1997; Wang *et al.*, 1997; Hu *et al.*, 2003; Chen *et al.*, 2011; Lai *et al.*, 2014).

The study of ER-shaping proteins in *Plasmodium* is of interest because the parasite's cell biology has several unique aspects linked to its parasitic life cycle and evolutionary position as an early-branching eukaryote. *Plasmodium*'s intracellular niche requires miniaturization of subcellular structures that could require specific membrane-curvature proteins. *Plasmodium* contains specialized organelles (micronemes, rhoptries, and dense granules) adapted to its host-cell invasion process, a plastid-like organelle (apicoplast) and forms a tubulovesicular network within the host cell (Bannister *et al.*, 2000; Hanssen *et al.*, 2008). Its erythrocytic stages also contain a hemoglobin-digesting digestive vacuole. Proteins trafficked from the ER to these organelles, parasite plasma membrane, parasitophorous vacuole, and exported to the host-cell are essential for infection, immune evasion and transmission to the vector (reviewed in Ingmundson *et al.*, 2014; Spielmann and Gilberger, 2015). Consequently, maintenance of ER morphology is likely to be important for *Plasmodium* virulence. Therefore, we have investigated potential determinants of ER morphology in *Plasmodium*. Rodent-infective and human-infective *Plasmodium* species encodes three homologs of proteins that induce membrane curvature and form ER tubules in higher eukaryotes, YOP1, YOP1-like (YOP1L), and RTN1 (Sun *et al.*, 2016). The parasite encodes one homolog of the ATL GTPase family of proteins, SEY1 (Sun *et al.*, 2016). No close homologs of Lnp have been found in the *Plasmodium* genome.

The three putative *Plasmodium* tubule-forming proteins have distinct transcriptomic expression profiles during *Plasmodium falciparum*'s asexual cycle (plasmoDB.org), which suggests that their functions could be nonredundant. The primary structures of YOP1, YOP1L, and RTN1 are highly conserved among rodent and human *Plasmodium* species (71%–73% identity in amino acid sequence) implying a fundamental role for the proteins regardless of their specific mammalian host. In previous work, we showed that *Plasmodium berghei* YOP1 (*PbYOP1*) when reconstituted into liposomes induces high membrane curvature consistent with tubule formation (Sun *et al.*, 2016) and its heterologous expression in *Saccharomyces cerevisiae* lacking the yeast homolog of YOP1 rescues ER shape (Sun *et al.*, 2016). Here, we use a genetic knockout of *PbYop1* (*Pbyop1Δ*) to functionally characterize the protein's role through the parasite's mammalian cycle.

FIGURE 1 Expression of *PbYOP1* and generation of knockout parasites. (a) *PbYOP1* was localized to the ER in asexual stages using co-staining with specific antibodies against YOP1 and an ER luminal protein, BiP1. (b) *PbYOP1* expression in sporozoites in perinuclear. CS is a marker for the sporozoite plasma membrane. (c) *PbYOP1* was not detected in liver stages formed in HepG2 cells 48 hr p.i. infected with sporozoites. (d) *Pbyop1* was replaced with an expression cassette for DHFR-ycfu using double homologous recombination. (e) Southern hybridization to confirm the modification of the *Pbyop1* locus in two independent *Pbyop1*Δ clones. (f) Western blotting to detect *PbYOP1* protein in asexual stages of WT parasites and two independent *Pbyop1*Δ clones, using anti-*PbYOP1* polyclonal sera. The arrow indicates full length *PbYOP1* protein and the star indicates cross-reacting bands. (g) Indirect immunofluorescence assays confirm the loss of *PbYOP1* protein in asexual stages and sporozoites of *Pbyop1*Δ clone 1.



2 | MATERIALS AND METHODS

2.1 | Ethics statement

All animal work in this project was approved by either the Institutional Animal Care and Use Committee (IACUC) of Tianjin Medical University (TMU), and was performed in accordance with ethical standards in Laboratory animal--Guideline for Ethical Review of Animal Welfare (The National Standard of the People's Republic of China GB/T 35892-2018) or by the IACUC of Rutgers New Jersey Medical School.

2.2 | Experimental animals and parasites

Male Wistar rats weighing 50–70 g and female BALB/c mice aged 4–6 or 6–8 weeks were purchased from Laboratory Animal Center of

Academy of Military Medical Sciences. Female C57BL/6 mice aged 6–8 week were purchased from SPF (Beijing) Biotechnology Co., Ltd. These animals were bred and housed at animal facility of TMU. Swiss-Webster mice (female, 6–8 weeks) were purchased from Taconic Biosciences. *P. berghei* ANKA lines were used in all experiments. Blood-stage *P. berghei* ANKA parasites were stored in liquid nitrogen. Parasitemia of infected mice was detected by Giemsa-stained thin smears from tail blood. At least 170–190 RBCs/field×20 fields were examined, for each sample, on an Olympus CX22 microscope with a 100×/1.25 oil immersion objective.

2.3 | Generation of *Pbyop1*Δ parasites

Plasmid *PbGEM-272858* designed to disrupt *PbYOP1* (PBANKA_0414500) in *P. berghei* genome was obtained from the *Plasmodium* Genetic Modification Project (Wellcome Trust Sanger

Institute - *PlasmoGEM* team, Cambridgeshire, UK). *PbGEM-272858* contains a 3×HA-dhfr-γFCU cassette flanked by 6607 and 1869 bp sequences from 5' and 3' end of the *yop1* coding sequence. NotI linearized *PbGEM-272858* was used to transfect *P. berghei* ANKA schizonts according to standard methodology (Janse *et al.*, 2006). The transfected parasites (*PbYOP1Δ*) were selected using pyrimethamine and cloned by limiting dilution. Genotype of the screened parasites were identified by Southern blotting and Western blotting.

2.4 | Southern blotting

Genomic DNA (gDNA) were extracted from the parasite pellets by QIAamp DNA Mini Kit (QIAGEN). Four microgram gDNA was digested with NdeI & KpnI (*PbYOP1Δ* parasite) or SwaI (WT + *yop1* parasites and *PbYOP1Δ* + *yop1* parasites) overnight at 37°C. The digested gDNA was separated on 0.8% of agarose gel and transferred to a positively charged nylon membrane (Roche). The nylon membrane was hybridized overnight at 55°C with ~1 kb probe labeled with DIG-dUTP by DIG High Prime DNA Labeling and Detection Starter Kit II (Roche). Detailed strategies of Southern blotting are displayed in Figure 1d and Figure S1a, and primers used for probe amplification are listed in Table S3.

2.5 | Preparation of anti-*PbYOP1* antibody

Rabbits were immunized with a combination of three *PbYOP1* peptides (NEKPSNEPPIKQDS-C, C-GNIAEKLVQEGVRRRN, and C-DLSGKLEQVDEYLKK). The polyclonal anti-*PbYOP1* sera was prepared by GL Biochem (Shanghai) Ltd.

2.6 | Western blotting

Western analysis of *PbYOP1* expression of *Pb* ANKA, *PbYOP1Δ*, and *PbYOP1Δ* + *yop1* parasites at asexual blood-stage were performed according standard methods. In brief, *P. berghei*-infected rat with a ~5% parasitemia was bled by cardiac puncture under terminal anesthesia. Blood was washed twice by RPMI 1,640 and 1×PBS (phosphate-buffered saline). Parasite pellets were obtained by erythrocytes lysis with NH₄Cl. After washed twice with PBS, the parasites were resuspended in lysis buffer (50 mmol/L Tris pH 7.5, 150 mmol/L NaCl, 1% Triton X-100, and protease inhibitor cocktail [Roche]) for ultrasound pyrolysis. The quantities of parasites total protein were adjusted by equal infected red blood cell (iRBC) numbers or equal amount of protein quantified by BCA Protein Assay Kit (Thermo Fisher Scientific). Approximately 4×10⁸ iRBCs protein extract or 5 μg protein of each sample were heated at 65°C in 6×protein sample loading buffer, electrophoresed on a 15% of SDS-PAGE gel, and transferred to a 0.45 μm PVDF membrane (Roche, Basel, Switzerland). Ponceau S staining of PVDF membrane was performed as a loading control. After staining, membranes were washed with

water, and then, blocked for 2 hr in 1×PBST (1×PBS containing 0.1% Tween 20) containing 5% of milk, and incubated with rabbit anti-*PbYOP1* antibody at a 1:1,000 dilution in 5% of milk overnight at 4°C. Bound antibodies were detected with a HRP-conjugated goat anti-rabbit IgG antibody (Invitrogen) diluted at 1:5,000 and ECL Western detection reagents (Merck).

2.7 | Transmission electron microscopy

TEM samples were processed one of two ways. Infected RBCs were fixed in 2% of paraformaldehyde/2.5% of glutaraldehyde (Polysciences Inc.) in 1×PBS, pH 7.2 for 1 hr at RT. Samples were washed in sodium cacodylate buffer at room temperature and postfixed in 1% of osmium tetroxide (Polysciences Inc.) for 1 hr. Samples were then rinsed extensively in water prior to en bloc staining with 1% of aqueous uranyl acetate (Ted Pella Inc.) for 1 hr. Following several rinses in water, samples were dehydrated in a graded series of ethanol and embedded in Eponate 12 resin (Ted Pella Inc.). Sections of 95 nm were cut with a Leica Ultracut UCT ultramicrotome (Leica Microsystems Inc.), stained with uranyl acetate and lead citrate, and viewed on a JEOL 1,200 EX transmission electron microscope (JEOL USA Inc.) equipped with an AMT 8 megapixel digital camera and AMT Image Capture Engine V602 software (Advanced Microscopy Techniques).

Infected RBC were washed thrice with cold PBS and fixed in 2.5% of glutaraldehyde in 0.1 M of sodium cacodylate buffer (pH 7.4) for 1 hr at RT, and resuspended in 0.1 M of sodium cacodylate buffer overnight. Cells were then postfixed for 1 hr in 1% of osmium tetroxide (Electron Microscopy Sciences) in the same buffer at room temperature, washed in water and stained for 1 hr at room temperature in 2% of uranyl acetate (Electron Microscopy Sciences), and then, washed again in water and dehydrated in a graded series of ethanol. The samples were then embedded in Embed-812 epoxy resin (Electron Microscopy Sciences). Ultrathin (50–60-nm) sections were cut using an Ultracut ultramicrotome (Reichert-Jung) and collected on formvar- and carbon-coated nickel grids, stained with 2% of uranyl acetate and lead citrate before examination with a Philips/FEI BioTwin CM120 electron microscope under 80 kV.

2.8 | Mosquito infections

Anopheles stephensi mosquitoes were fed on infected Swiss-Webster mice. Mosquitoes were maintained on 20% of sucrose at 25°C at a relative humidity of 75%–80%. Sporozoites were obtained by crushing salivary glands dissected on days 18–25 postfeeding.

2.9 | Immunofluorescence assays for protein detection in sporozoites and asexual stages

Primary antibodies used were: anti-YOP1 (1:1,000), anti-*P. berghei* BiP1 ([Kaiser *et al.*, 2016] 1:500, a kind gift of Dr. Rebecca Stanway),

anti-*P. falciparum* BiP1 (1:500, a kind gift of Dr. Kasturi Halder), and anti-CS (3D11, 1 µg/ml). Secondary antibodies (anti-rabbit Alexa488 and anti-mouse, Molecular Probes) were used at a dilution of 1:3,000.

Infected RBCs were washed twice in PBS for 5 min with gentle mixing. They were fixed in 4% of paraformaldehyde for 30 min at RT and permeabilized with cold methanol for 15 min at RT. Methanol was removed by washing with PBS. Cells were blocked in 3% of BSA/PBS for 1 hr at RT before addition of the primary antibody diluted in blocking buffer. Cells were incubated, with gentle rotation, either overnight at 4°C or at RT for 2 hr. After three washes with PBS, 5 min each, secondary antibody was added for 1 hr at RT. Cells were thrice washed in PBS before being spread on a glass slide.

Sporozoites ($0.5-1 \times 10^6$) were purified as previously described (Kennedy *et al.*, 2012), air-dried at room temperature on poly L-lysine coated glass slides. They were fixed in 4% of PFA for 20 min at RT, permeabilized with 0.5% of Triton X-100 for 15 min at RT before blocking with 3% of BSA in PBS for 1 hr. Primary antibodies diluted in blocking solution were added at the appropriate dilutions and incubated either for 1 hr at RT or overnight for 4°C. Secondary antibodies diluted in blocking solution were incubated for 1 hr at RT. Washes with PBS were performed after incubation with each antibody.

2.10 | Determination of sporozoite motility, invasion and liver stage development

For measuring motility at day 18 post blood-meal, sporozoites dissected in plain DMEM (1×10^4) were transferred to a 96-well plate with an optical bottom, together with an equal volume of 6% BSA. They were centrifuged for 3 min at 4°C and filmed on a Nikon A1R laserscanning confocal microscope using a 20×/NA0.75 objective at 37°C. Movies were recorded over 90 frames at 1 Hz. Image acquisition and analysis was performed using NIS Elements software from Nikon. Movement patterns and the number of circles executed by gliding sporozoites were determined through visual inspection of individual sporozoites.

For measuring invasion, sporozoites dissected in DMEM supplemented with 10% of FCS medium (4×10^4 /well, 150 µl/well) were added to confluent HepG2 cells plated in 8-chamber LabTek slides. Invasion assays were performed as previously described (Sinnis *et al.*, 2013). Briefly, cells were fixed with 4% of PFA at 90, 120 and 180 min after sporozoite addition. They were blocked with 3% of BSA in PBS and incubated with 3D11 (1 µg/ml) for 1h at RT. After washes with PBS, cells were incubated with anti-mouse Alexa594 (1:3,000) for 1 hr at RT. Cells were permeabilized with cold methanol for 15 min, blocked and incubated with 3D11. After washes, cells were incubated with anti-mouse Alexa488 (1:3,000) for 1 hr at RT. The number of sporozoites that became intracellular were determined by calculating the difference in numbers of sporozoites that stain with Alexa488 and Alexa594. The percentage of sporozoites that invaded was calculated by determining the percentage of total sporozoites that were intracellular.

For measuring intrahepatic development, sporozoites ($2-4 \times 10^4$ /well) dissected in DMEM supplemented with 10% of FCS, were added

to HepG2 cells plated in 8-chamber LabTek slides. To determine its effect on liver stage development, IAA or vehicle was added to infected HepG2 cells 3 hr p.i. Medium was replaced at 14 hr p.i. and cells fixed for immunofluorescence analysis using anti-HSP70 as described above.

2.11 | Determination of multiplication rate and parasite growth in the erythrocytic cycle

The *in vivo* multiplication rate of asexual blood-stage was determined as described before (Spaccapelo *et al.*, 2010). The parasitemia of BALB/c mice (4–6 weeks) infected with a single infected erythrocyte was determined by counting Giemsa-stained blood smears when parasitemia reached 0.5%–2%. The mean asexual multiplication rate per 24 hr was calculated assuming a total of 1.2×10^{10} erythrocytes/mouse (2 ml of blood).

To determine the effect of *Pbyop1* disruption on asexual parasite growth *in vivo*, WT- or *Pbyop1Δ*-infected erythrocytes (20 and 200) were injected intravenously into Wistar rats (male, 50–70 g, 4–5 rats/group). Parasitemia was monitored daily for 12 days, using Giemsa staining. To determine the effect of *Pbyop1* disruption on the sexual cycle, Swiss-Webster mice (female, 6–8 weeks) were intravenously injected with WT- or *Pbyop1Δ*-infected erythrocytes (200 µL, 1% parasitemia) at $d = 0$. Gametocytes were counted at $d = 3$, using Giemsa-stained blood smears.

2.12 | Hemozoin quantification

Quantification of hemozoin in WT and *Pbyop1Δ* parasites were performed as previously described (Pisciotta *et al.*, 2017). Blood from a donor BALB/c mouse at ~1% parasitemia was transferred to four mice. These mice were sacrificed at ~1% parasitemia ($n = 4$ mice/group). The blood volumes of each mouse in two groups were normalized by iRBC count. About 500 µl of blood of each mouse was hypotonically lysed in 4.5 ml of H₂O, centrifuged at 14,000 g for 15 min. Pellets were resuspended in 1 ml of 2% SDS, 100 mM NaHCO₃ (pH 9.0), spun at 14,000 g for 15 min, washed in 2% of SDS and centrifuged again as above. Washed pellets were incubated in 1 mg/ml of proteinase K buffer overnight at 60°C. After protease treatment, samples were washed in H₂O, and centrifuged as above to purify hemozoin. Finally, the purified hemozoin pellets were solubilized in 1 ml of 2% SDS with 20 mM of NaOH at room temperature for 1 hr. Optical density (OD) was measured at 405 nm using a Multiskan Spectrum (Thermo Scientific). A standard curve was generated with 2-fold dilutions of 1 mM heme (H9039; Sigma-Aldrich) in DMSO.

2.13 | Yeast strains and plasmid

The following *S. cerevisiae* strains were used: BY4741 (*MATa his3Δ1 leu2Δ met15Δ ura3Δ*), NDY257 (*BY4741 rtn1Δ::kanMX4 rtn2Δ::kanMX4*

yop1Δ::kanMX), JHY1 (BY4742 *yop1Δ::HIS3MX6*), JHY2 (BY4742 *rtn1Δ::HIS3MX6*), and JHYO (BY4741 *sey1Δ::kanMX4*). To visualize yeast vacuole, the vacuolar membrane marker Vph1 (V-type proton ATPase subunit a) was used. The full coding region of Vph1p plus a C-terminal GFP tag was amplified and inserted into the BamHI/HindIII site of pRS316 (a URA3/CEN plasmid). 310 bp upstream and 319 bp downstream sequences of Vph1p was amplified and inserted into the NotI/XbaI and HindIII/XhoI sites of the above resulting plasmid. Primers used for construction of pRS316-VPH1-GFP are listed in Table S3. Yeast transformation (introducing pRS316-VPH1-GFP into the yeast strains mentioned above) was accomplished according to standard procedures.

2.14 | Fluorescence microscopy of yeast

Yeast cells were imaged live at room temperature using a Leica TCS SP5 confocal microscope with a 63×/1.40 N.A. Plan Apochromat oil immersion objective lens using LAS AF (version 1.3.1 build 525) software. Yeast cells were classified into three classes according to the morphology and numbers of the vacuoles labeled with Vph1-GFP (Frohlich *et al.*, 2015). Cells with 1–3 vacuoles were designated as Class I, cells with multiple round vacuoles were designated as Class II and cells with no round vacuolar structures were designated as Class III.

2.15 | Experimental cerebral malaria model and assessment

C57BL/6 mice (female, 6–8 weeks) were infected i.v. with 1×10^4 WT, 1×10^4 or 1×10^6 Pbyop1Δ parasites. They were monitored daily for signs of disease, classified into five clinical stages as previously described (Villegas-Mendez *et al.*, 2012): 1 = no signs; 2 = ruffled fur/abnormal posture; 3 = lethargy; 4 = reduced responsiveness to stimulation/ataxia/respiratory distress/hyperventilation; 5 = prostration/paralysis/convulsions. Mice were classified as exhibiting ECM at stage 4/5.

2.16 | Blood–brain barrier permeability

To assess the integrity of the BBB, C57BL/6 mice at stage 4/5 were injected intravenously with 200 μl of 2% Evans Blue solution (in 1×PBS, pH 7.2). One hour after injection, mice were euthanized and perfused transcardially with 40 ml 1×PBS. The brain of each mouse was dissected out and weighed, and then, incubated in 1 ml of formamide (Solarbio, Beijing, China) for 48 hr at 37°C. The optical density (OD) value of extracted Evans Blue dye in the solution were measured using a spectrophotometer at 630 nm. Evans Blue extravasation of the brain was calculated as Evans Blue dye (mg)/brain tissue (g) based on a standard curve.

2.17 | Tissue processing

For histopathology studies, C57BL/6 mice were transcardially perfused with 40 ml 1×PBS after final anesthesia. The brain of each mouse was dissected out and cut along the mid-sagittal line, and fixed in 4% of PFA for 24 hr at room temperature. Then, the PFA fixed brain tissues were dehydrated through an ethanol gradient, incubated with molten paraffin wax, then embedded and allowed to cool. Finally, the PFA fixed, paraffin embedded (PFPE) tissues were serially sectioned at a thickness of 4 μM along the sagittal plane (interaural), so the entire brain structure could be visualized. The brain sections were analyzed via hematoxylin and eosin (H&E) staining or immunohistochemistry.

2.18 | Determination of cerebral histology

To assess the degree of hemorrhage and microvascular obstruction in brain tissue, the PFPE brain sections were analyzed by H&E staining. The image was visualized at 10× or 40× objectives and captured on a Nikon ECLIPSE 90i microscope using NIS-Elements BR (version 3.1) software. The entire sagittal section of the brain was visualized and its area calculated. The number and area of hemorrhages and the number of microvascular obstructions were averaged over the entire sagittal section.

2.19 | Statistical analyses

For comparing between two groups, statistical significance was analyzed using Mann–Whitney *U* test or unpaired two-tailed *t* test. One-way ANOVA with Tukey's test or Kruskal–Wallis ANOVA test was used to compare multiple groups. Two-way ANOVA followed by Tukey's multiple comparisons was performed to compare multiple groups with two independent variables. Cumulative survival rates of the mice among different groups were assessed using Kaplan–Meier method and compared using log-rank test. All data were analyzed by GraphPad Prism software (version 6.0c). *p* < .05 was considered statistically significant. **P* < .05, ***P* < .01, ****P* < .001, *****P* < .0001, ns, not significant.

3 | RESULTS

3.1 | PbyOP1 function is crucial for parasite virulence in the erythrocytic cycle

To examine the expression of PbyOP1, we raised specific polyclonal sera and used it to examine the spatial expression of PbyOP1 in erythrocytic stages and sporozoites using indirect immunofluorescence assays. In asexual stages, PbyOP1 is present in subcellular structures consistent with the peripheral ER. As observed with yeast and mammalian homologs (Voeltz *et al.*, 2006), PbyOP1 partially co-localizes with a pan-ER marker BiP1, a protein resident in the ER

lumen (Figure 1a). In sporozoites, *PbYOP1*'s localization is primarily perinuclear, consistent with ER localization (Figure 1b). *PbYOP1* was not detectable in liver stages 48 hr postinfection (Figure 1c). To functionally characterize *PbYOP1*, we generated a gene knockout (*Pbyop1* Δ) using double homologous recombination (Figure 1d,e). Protein loss in *Pbyop1* Δ parasites was confirmed through Western blotting and immunofluorescence assays (Figure 1f,g). As a control, we generated complemented parasites in which the *PbYop1* gene and protein expression was restored (Figure S1a-f).

Two independent *Pbyop1* Δ clones were examined for growth during the erythrocytic cycle and were found to be highly attenuated in the erythrocytic cycle. WT-infected mice developed microscopically-detectable parasitemia 1–2 days (depending on the dose) prior to *Pbyop1* Δ -infected mice (Figure 2a). *Pbyop1* Δ parasites have a multiplication rate of \sim 7-fold over 24 hr (Table S1) compared to 10-fold for WT parasites (Janse *et al.*, 2003; Spaccapelo *et al.*, 2010). Our results confirm those obtained in a genome-wide gene-knockout study that found *Pbyop1* Δ parasites to be slow growing (Bushell

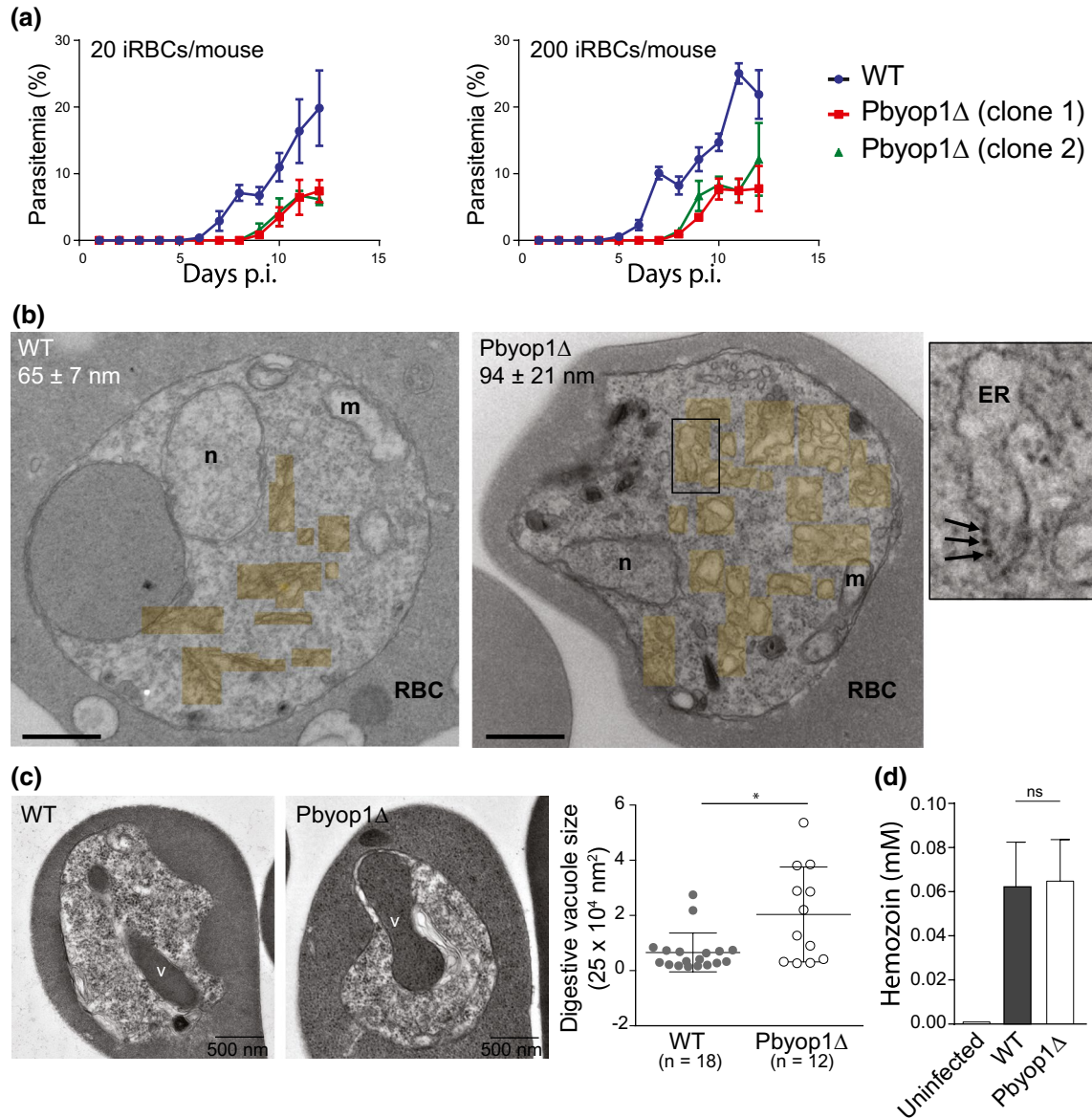


FIGURE 2 Loss of *PbYOP1* leads to aberrant ER morphology and digestive vacuole, and attenuated growth. (a) Growth curves of WT and two independent clones of *Pbyop1* Δ parasites in rats ($n = 4$ – 5) reveal that *PbYOP1*'s deletion reduces parasite fitness in the asexual cycle. Data shown are from one experiment representative of three independent experiments. Data are mean \pm SD and were analyzed by two-way ANOVA followed by Tukey's multiple comparisons. WT versus *Pbyop1* Δ clone 1/clone 2, $p < .0001$. (b) Ultrastructure of infected RBC with the parental or KO strain. Parasite ER is pseudocolored in yellow. ER was identified based on the presence of ribosomes (arrows) on the limiting membranes (enlarged area indicated by black box). The mean diameters of ER elements are shown. n, nucleus; m, mitochondrion. Bars, 500 nm. (c) Representative images of TEM sections showing digestive vacuoles (v) in WT and *Pbyop1* Δ parasites and quantification of vacuole size. Data are mean \pm SD and were analyzed by unpaired *t* test with Welch's correction. * $p = .05$. (d) Hemozoin was quantified in WT and *Pbyop1* Δ parasites. Data shown are representative of three independent experiments. Data are mean \pm SD and were analyzed by unpaired two-tailed *t* test. ns, not significant

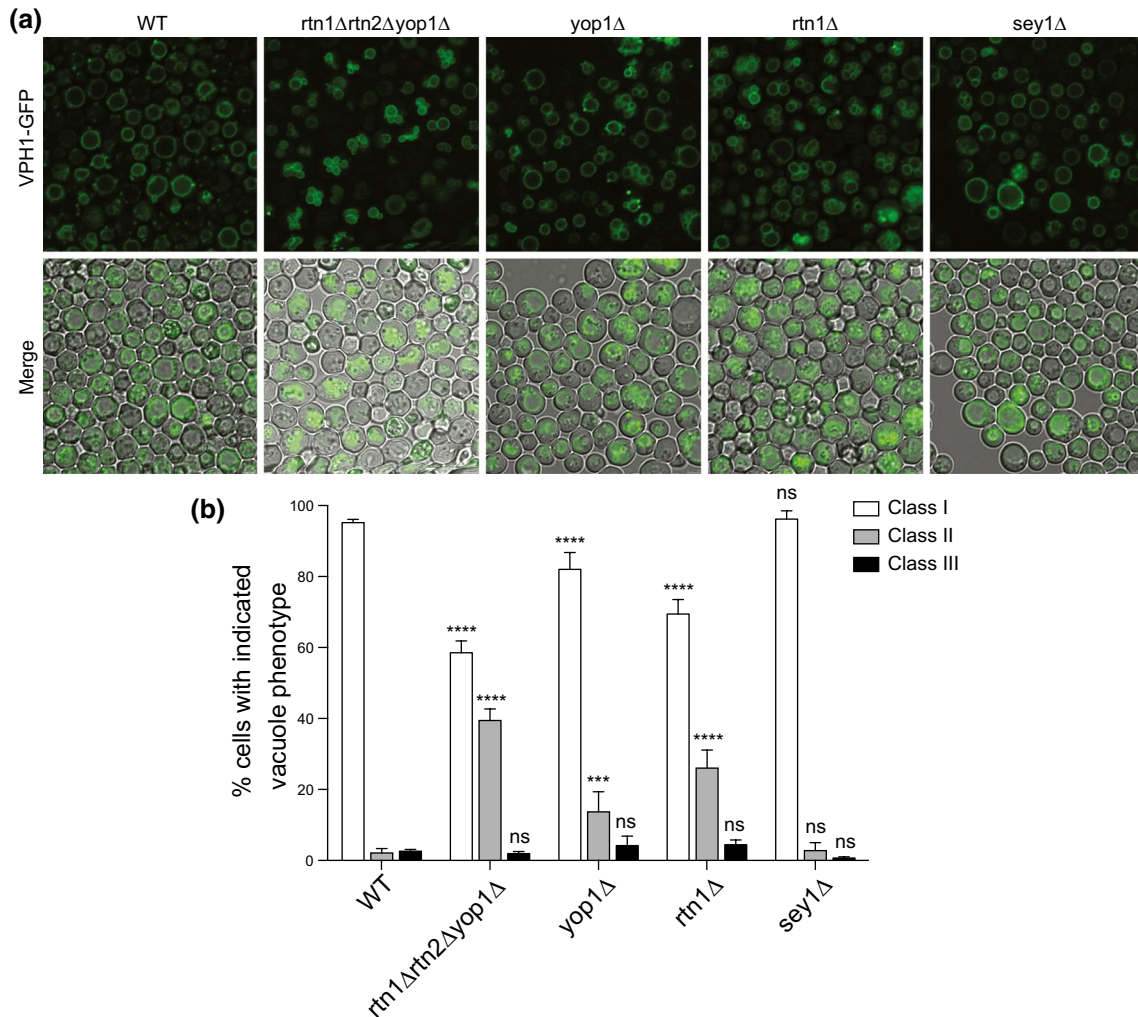


FIGURE 3 Vacuole morphology in *Saccharomyces cerevisiae* mutants of *Pbyop1* homologs (*ScRtn1p*, *ScRtn2p*, *ScYop1p*) was determined using a vacuole marker. (a) Immunofluorescence images of vacuoles in *S. cerevisiae* lacking ER-shaping proteins. Vacuoles were visualized using anti-VPH1. Individual yeast cells were categorized according to the number of vacuoles they contained. (b) Yeast cells with class I, class II, and class III vacuoles are shown as a percentage of the total number. Cells with 1–3 vacuoles were designated as Class I, cells with multiple round vacuoles were designated as Class II and cells with no round vacuolar structures were designated as Class III. At least 50 cells were counted in each yeast strain. Data shown are mean \pm SD and representative of three independent experiments. Two-way ANOVA with Tukey's multiple comparison test was performed to compare the percentage of each class in mutant and WT strain. *** $p < .001$, **** $p < .0001$, ns, not significant

et al., 2017). The delay in growth of *Pbyop1Δ* could be rescued completely through complementation with *Pbyop1* (Figure S1g, left panel). We also noted that a significantly higher proportion ring/early trophozoite-stage parasites in *Pbyop1Δ*-infected mice (Figure S1g, right panel), suggesting that *PbYOP1* may be required for the transition from ring to trophozoite. We conclude that that *PbYOP1* plays a critical role during the asexual cycle.

3.2 | YOP1 proteins may play an evolutionarily conserved role in maintaining ER and vacuole morphology

We examined the ultrastructure of *Pbyop1Δ* parasites using transmission electron microscopy (TEM; Figure 2b). TEM revealed that

ER tubules are significantly enlarged in *Pbyop1Δ* compared to WT parasites (Figure 2b). Representative electron micrographs, from WT ($n = 28$) and *Pbyop1Δ* ($n = 39$) parasites were selected for quantitative morphometric analysis of ER diameters and analyzed as previously described using the standard formula for randomly oriented cell and structures (Oppenroes *et al.*, 1984). All images were at the same magnification to ensure that the entire parasite fit into the field of view. The mean diameter of the ER was 65 ± 7 nm for WT parasites ($n = 15$) and 94 ± 21 nm for mutant parasites ($n = 29$). These results confirmed that deletion of *PbYOP1* alters ER morphology. EM results also demonstrated that *Pbyop1Δ* parasites were typically at the “ring” stage, with the cytotome attached to the erythrocyte cytoplasm (Figure S2a). A large proportion of parasites in the *Pbyop1Δ* sample had a vacuolated appearance, consistent with them dying (Figure S2b). We postulate that the erythrocytic cycle

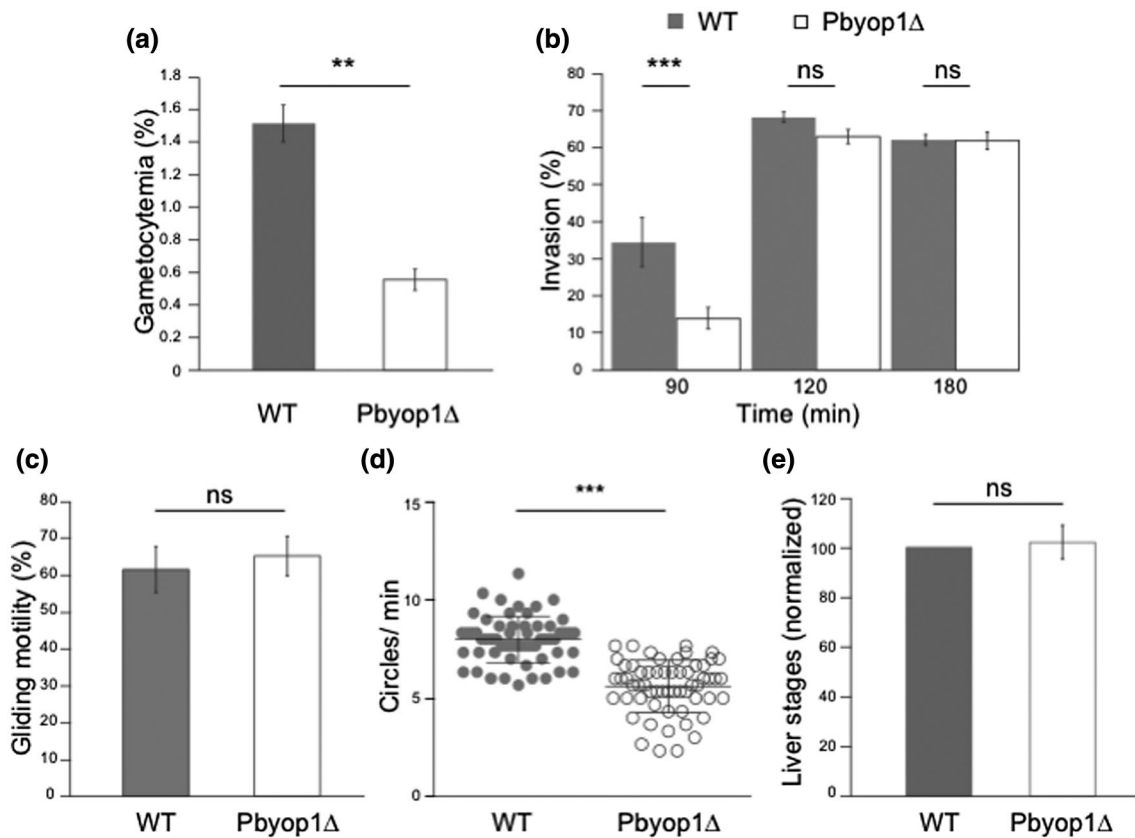


FIGURE 4 Characterization of *Pbyop1Δ* in preerythrocytic stages. (a) Gametocytemia (mean \pm SEM) in mice infected with *Pbyop1Δ* parasites is significantly lower than in WT-infected mice. The experiment was performed twice ($n = 13$ – 14). (b) Invasion of HepG2 cells by *Pbyop1Δ* sporozoites is slower compared to WT. The percentage of sporozoites (\pm SD) that are intracellular was determined at 90, 120, and 180 min after addition to cells. The experiment was performed four times at 90 min and once at other time points, each with four technical replicates. (c) Deletion of *Pbyop1* does not affect sporozoite gliding in vitro. The percentage of sporozoites that displayed continuous circular motion (\pm SD) was determined using live imaging ($n \geq 600$). The experiment was performed once with two technical replicates. (d) Deletion of *Pbyop1* decreases the speed of sporozoite motility. Speed was quantified as the number of circles completed per minute by gliding sporozoites. (e) Deletion of *Pbyop1* does not affect the development of liver stages. The number of liver stages (\pm SEM) present in infected HepG2 cultures at 48 hr p.i. was determined. The experiment was performed thrice, each with four technical replicates. The number of liver stages formed by mutant sporozoites was normalized against WT (992 ± 2). Data in Figure 4 were analyzed by unpaired *t* test. ** $P < .01$, *** $p < .001$, ns, not significant

of *Pbyop1Δ* parasites is attenuated due to both reduced fitness and delayed ring-to-trophozoite transition, marked by the formation of the hemoglobin-degrading digestive vacuole. The digestive vacuole in *Pbyop1Δ* parasites ($50.9 \pm 12.4 \text{ nm}^2$) was significantly enlarged compared to WT parasites ($16.4 \pm 8.8 \text{ nm}^2$; Figure 2c) while there was no significant difference in parasite size ($475.1 \pm 45.1 \text{ nm}^2$ for WT and $486.4 \pm 48.0 \text{ nm}^2$ for *Pbyop1Δ*). We reasoned that the larger size of the digestive vacuole in mutant parasites could result from slower hemoglobin degradation. Therefore, we quantified the amount of hemozoin in *Pbyop1Δ* parasites. Total hemozoin amount was found to be similar in *Pbyop1Δ* and WT parasites (Figure 2d). Since heme release is thought to occur soon after hemoglobin is unraveled by the action of the aspartyl protease, plasmepsin 4 (Goldberg, 1993), normal levels of hemozoin in *Pbyop1Δ* parasites suggest that loss of *Pbyop1* does not abrogate early steps hemoglobin degradation. It is likely that later steps of hemoglobin degradation are affected leading to the increased size of the digestive vacuole.

Since loss of *Pbyop1* correlates with defects in digestive vacuole formation, we tested if its orthologs in higher eukaryotes also play a role in vacuole formation. *S. cerevisiae* contains a single large vacuole and encodes three *PbYop1* homologs, ScRTN1, ScRTN2, and ScYop1 (Hu *et al.*, 2011). ScRTN1 and ScYop1 are relatively abundant, whereas ScRTN2 expresses at a low level. We monitored vacuole morphology in *S. cerevisiae* mutants lacking either ScYop1 or ScRTN1, and a mutant lacking all three, using GFP-tagged V-type proton pump VPH1 as a vacuole membrane marker. When ScYop1p or ScRtn1p were deleted, a significant number of cells exhibited more than three vacuoles with a grape-like assembly (Figure 3). The vacuolar defect was further augmented in a triple mutant for ScYop1p, ScRtn1p, and ScRtn2p. The defect in vacuole morphology is specific to *PbYop1* homologs because there was no change in the number of vacuoles per cell when ScSey1p, a mediator of ER membrane fusion was deleted. These results suggest a possibly evolutionarily conserved role of YOP1-like proteins in regulating vacuole morphology.

3.3 | *PbYOP1* plays a major role in parasite transmission from host to vector

Next, we examined the ability of *Pbyop1Δ* parasites to transmit from the mammalian host to mosquitoes by quantifying the number of male and female gametes in infected mice and the average number of oocysts in midguts of infected mosquitoes that fed on these mice. The average gametocytemia for *Pbyop1Δ* ($0.55 \pm 0.06\%$, $n = 13$ mice) was significantly lower than WT ($1.51 \pm 0.11\%$, $n = 14$ mice; Figure 4a) and at least partially accounts for the dramatic decrease in the number of midgut oocysts (WT: 11 ± 2 , $n = 10$; *Pbyop1Δ*: 1 ± 1 , $n = 10$) and salivary glands sporozoites recovered from *Pbyop1Δ*-infected mosquitoes (WT: $17,929 \pm 964$ sporozoites/mosquito, $n = 280$; *Pbyop1Δ*: $2,230 \pm 174$ sporozoites/mosquito, $n = 700$). These results demonstrate that *PbYOP1* is required for natural transmission of the parasite from the mammalian host to the mosquito vector.

To test if *PbYOP1* functions in sporozoites, as might be implied by its expression, we examined the ability of *Pbyop1Δ* sporozoites to invade the hepatoma cell line, HepG2. Sporozoite invasion was measured, at 90, 120 and 180 min, by quantifying the percentage of sporozoites that become intracellular in the test period. *Pbyop1Δ* sporozoites displayed a brief delay in invasion--at 90 min their invasion rate was ~50% of WT. By 120 min, there was no significant difference in the invasion rate of *Pbyop1Δ* and WT sporozoites (Figure 4b). Next, we determined if the delay in invasion resulted from aberrant sporozoite motility. For this, we observed the movement patterns of live sporozoites on glass coverslips to determine the fraction of sporozoites that demonstrated continuous circular motion (gliding motility; Hegge *et al.*, 2009). As a proxy for speed of movement, we quantified the average number of circles completed by gliding sporozoites in the observation period (Hegge *et al.*, 2010). The percentage of *Pbyop1Δ* sporozoites that displayed continuous circular motion was same as WT but the average number of circles per minute was significantly reduced to 5.6 ± 0.6 ($n = 59$) from 7.9 ± 0.5 for WT ($n = 59$; Figure 4c-d).

After entering the hepatocyte, sporozoites undergo a differentiation program that eventually leads, through schizogony, to the generation of tens of thousands of liver stage forms. The conversion of a single sporozoite to liver stages requires membrane biogenesis, a process that depends on phospholipid biosynthesis in the ER. As liver stage development proceeds, the parasite ER and plasma membrane interact closely at several membrane contact sites (Burda *et al.*, 2017). To determine if the parasite's differentiation from sporozoite to liver stages requires *PbYOP1* function, *Pbyop1Δ* sporozoites were allowed to infect HepG2 cells, as a proxy for their ability to infect the mammalian liver. There was no significant difference in the number of liver stages formed by *Pbyop1Δ* or WT parasites (Figure 4e) at 48 hr p.i. We were unable to interrogate the subsequent step of maturation of liver stages into hepatic merozoites because of the low numbers of *Pbyop1Δ* sporozoites available.

To determine the effect of *PbYOP1* function on infectivity *in vivo*, mice were infected through intravenous injection of 5×10^3

WT or *Pbyop1Δ* sporozoites. They were monitored daily for the appearance of microscopically detectable blood-stage parasites. The average prepatent period of WT sporozoites was 3.4 ± 0.3 days. *Pbyop1Δ*-infected mice were monitored for 3 weeks but none of them became positive. When mice were infected with *Pbyop1Δ* parasites through mosquito bite, they developed blood-stage parasitemia (data not shown). Since bite infections are not quantitative, we could not establish if *Pbyop1Δ* sporozoites are compromised during natural transmission as they are during intravenous injection. Nevertheless, these data established that *PbYOP1* plays an important function during the preerythrocytic cycle. The diminished infectivity of *Pbyop1Δ* sporozoites *in vivo*, revealed through intravenous infection, may be attributed partly or wholly to delayed invasion caused by their slower motility observed *in vitro*.

3.4 | Deletion of *PbYOP1* inhibits experimental cerebral malaria pathogenesis

Cerebral malaria is a severe neurological complication that is responsible for the majority of malaria-related deaths (World Health Organization, 2019). It is associated with sequestration of *P. falciparum*-infected erythrocytes in the brain (Storm and Craig, 2014) mediated by parasite proteins exported to the erythrocyte surface. The vacuole defects suggested that *PbYOP1*'s loss could impact trafficking and ER export of parasite proteins during the asexual cycle. Therefore, we investigated what effect its loss has on parasite virulence.

We assessed the ability of *Pbyop1Δ* parasites to induce experimental cerebral malaria (ECM) in C57BL/6 mice intravenously inoculated with WT- or *Pbyop1Δ*-infected erythrocytes (1×10^4 iRBC/mouse). All WT-infected mice displayed signs of ECM (stage 4/5; Villegas-Mendez *et al.*, 2012) and died within 7–9 days p.i. with peripheral parasitemia ranging from 5% to 8% at day 7 p.i. (Figure 5a,b, Table S2). In contrast, at day 7 p.i., 97% of *Pbyop1Δ*-infected mice were alive and did not display signs of ECM (Figure 5a,b, Table S2). In order to eliminate parasitemia-linked differences in ECM, arising from the mutant's slower growth rate, we tested a higher infectious dose of *Pbyop1Δ* (1×10^6 iRBC/mouse). In this case, 9% of mice infected with 1×10^6 *Pbyop1Δ* iRBCs died of ECM within day 6–11 p.i. (Figure 5a,b, Table S2). These mice had peripheral parasitemia similar to WT (Figure 5b) but 91% of them were alive at day 7 p.i., with no obvious signs of ECM (Figure 5a, Table S2). Restoration of *PbYOP1* expression in *Pbyop1Δ* parasites reverted mortality to 100%, similar to WT infection (Figure S1h). *Pbyop1Δ*-infected (1×10^4 or 1×10^6) mice eventually died from hyperparasitemia and severe anemia after day 20 p.i.

ECM demonstrates many features of cerebral malaria such as increased permeability of the blood–brain barrier (BBB), intracerebral hemorrhages and microvascular obstruction. In order to assess ECM-linked pathophysiological changes in WT- and *Pbyop1Δ*-infected mice, we recovered brain-tissue from WT-infected mice on day 7 p.i., when WT-infected mice displayed signs

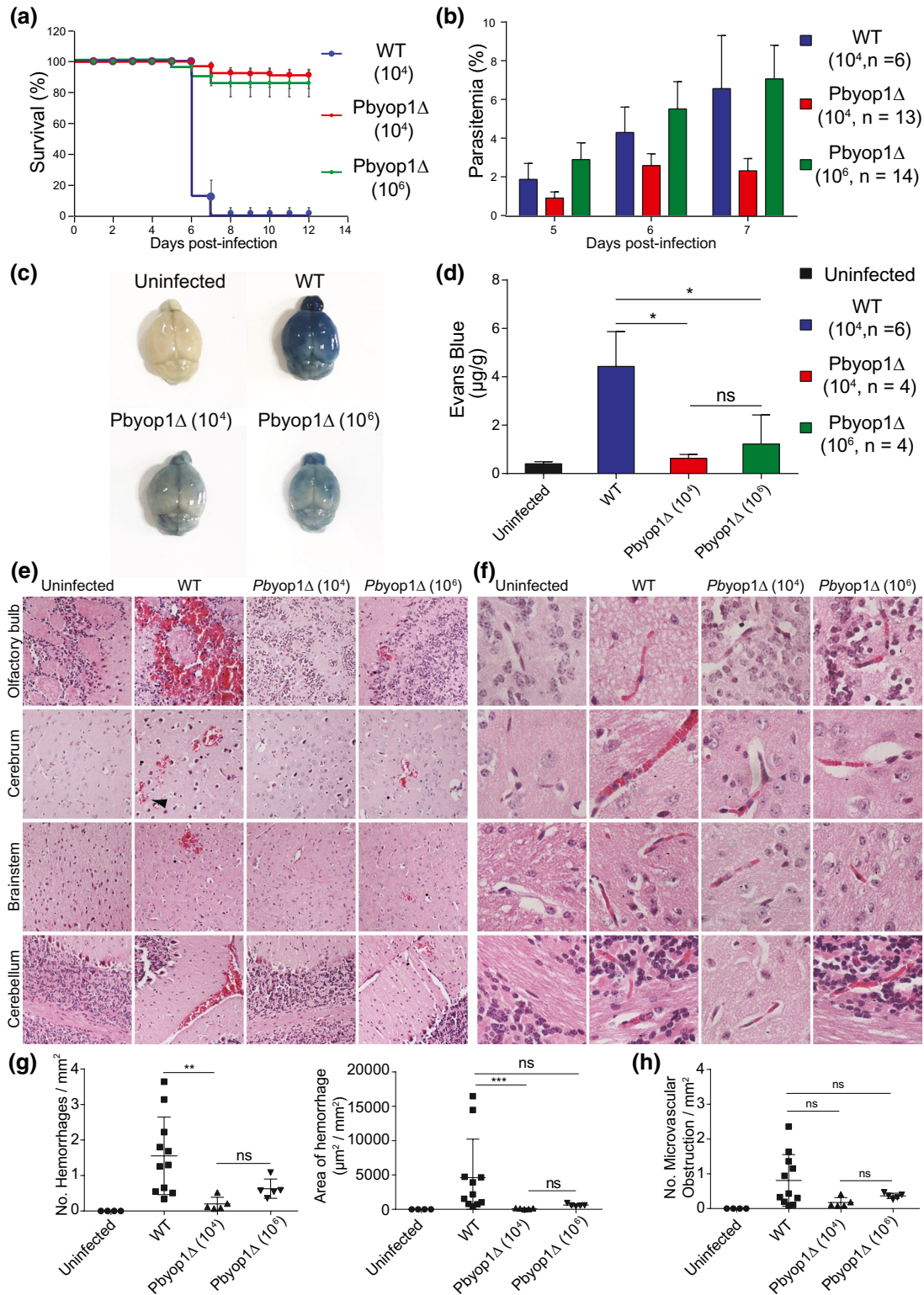


FIGURE 5 Loss of *PbYOP1* attenuates pathological manifestations of ECM. (a) Survival was significantly higher in *Pbyop1Δ*-infected mice than in WT-infected mice. Data shown are average of five independent infection experiments. (b) At day 7 postinfection, *Pbyop1Δ*-infected mice demonstrated peripheral parasitemia similar to mice infected with 100-fold fewer WT parasites. (c) Representative images of brains from mice infected with WT or *Pbyop1Δ* parasites, injected with Evans Blue to detect BBB leakage. (d) Quantification of Evans Blue in brains of mice demonstrating ECM. (e-f) Representative images of brain histopathology at day 7 p.i. from mice infected with WT or *Pbyop1Δ*. Hemorrhages in (e; arrowhead) and microvascular obstructions in (f; arrowhead) were observed in mice infected with either WT or 10⁶ *Pbyop1Δ* parasites. (g) Quantification of the numbers and areas of hemorrhages in (e). (h) Quantification of the numbers of microvascular obstructions in (f). Data are shown as mean ± SD (a, b, d, g, h) and were analyzed by Kruskal–Wallis ANOVA test (d, g, h). **p* < .05, ***p* < .01, ****p* < .001, ns, not significant

corresponding to stage 4/5 (classified as ECM). In contrast, on day 7 p.i., *Pbyop1Δ*-infected mice typically displayed signs corresponding to stage 1–3 (classified as non-cerebral malaria [NCM]). The number of *Pbyop1Δ*-infected mice that displayed ECM on day 7 p.i. was too low, and therefore, these mice were excluded from further analysis. Integrity of the BBB was examined using Evans Blue staining of brain tissue at day 7 p.i. Brains of WT-infected mice demonstrated greater permeability (Figure 5c,d) than of *Pbyop1Δ*-infected mice, consistent with their higher rates of ECM. WT-infected mice also demonstrated intracerebral hemorrhages and microvascular obstructions, predominantly in olfactory bulbs, brainstem, and cerebellum (Figure 5e,f). Mice infected with 10^4 *Pbyop1Δ* had minor pathological changes in the brain, consistent with NCM (Figure 5e,f). Greater number of hemorrhages and microvascular obstructions were observed on day 7 p.i. in mice infected with 10^6 *Pbyop1Δ* parasites but these were alleviated by day 11 p.i. (Figure S3). The resolution of pathology by day 11 p.i. in mice infected with 10^6 *Pbyop1Δ* parasites is consistent with the marked decrease in ECM-related deaths in this group compared to WT-infected mice (Figure 5g,h). No intracerebral hemorrhage and microvascular obstruction were observed in uninfected mice. These results demonstrate that loss of *Pbyop1* severely attenuates parasite virulence by decreasing its ability to induce ECM.

4 | DISCUSSION

PbYOP1's effect on virulence of asexual stages could result from interrupted development of the digestive vacuole and/or slower hemoglobin degradation within it. A proximal function in determining digestive vacuole morphology is supported by the phenotype of homologous *S. cerevisiae* mutants that we observed. Yeast cells lacking reticulons contain vacuoles with multiple lobes consistent with a block in fusion. Digestive vacuole biogenesis also requires fusion of endocytosed vesicles. Digestive vacuole biogenesis begins in early rings with endocytosis at a cytoskeletal ring structure on the parasite surface termed cytosome (Aikawa *et al.*, 1966; Dluzewski *et al.*, 2008; Lazarus *et al.*, 2008). Two models have been proposed to explain the next steps. One model postulates that several small cytosomal-derived vesicles containing hemoglobin eventually fuse together to form a single digestive vacuole that continues to receive vesicles containing endocytosed hemoglobin (Abu Bakar *et al.*, 2010). The other model suggests that a single cytosome invagination elongates into a tubule that pinches off from the plasma membrane and fuses immediately with the digestive vacuole. Both models involve vesicle biogenesis and trafficking that could be affected by structural changes in the ER. Hemoglobin within the digestive vacuole is digested by proteolytic enzymes trafficked from the parasite's secretory pathway (Klemba *et al.*, 2004). One explanation for the enlarged digestive vacuoles and normal hemozoin levels in *Pbyop1Δ* parasites is that dysmorphic ER in these parasites interferes with vesicle formation and trafficking of proteolytic enzymes to the developing digestive vacuole, slowing down hemoglobin degradation downstream of heme release.

This model is supported by phenotypes observed in mammalian cells missing homologs of *PbYOP1*. Neurons missing a *PbYOP1* homolog, REEP1, have abnormally large lysosomes (Allison *et al.*, 2017). Relevantly, the *Plasmodium* digestive vacuole is an endosome-lysosome-like compartment (Francis *et al.*, 1997). Additionally, consistent with a defect in protein trafficking in *Pbyop1Δ* parasites, mammalian cells with mutations in ER-shaping proteins experience a severe defect in COPII-coated vesicle trafficking from the ER to Golgi (Niu *et al.*, 2019). This likely explains the mislocalization of specific proteins in retinal photoreceptors of mutants lacking another *PbYOP1* homolog, REEP6, (Agrawal *et al.*, 2017; Veleri *et al.*, 2017).

A defect in secretion could also explain aberrant motility in *Pbyop1Δ* sporozoites. A recent model suggests that motility of *Toxoplasma gondii* tachyzoites requires a secretory-endocytic pathway of membrane fusion (Gras *et al.*, 2019). Vesicles fuse at the apical end and membrane is endocytosed at the posterior end giving rise to membrane-flow. If membrane-flow plays a major role in sporozoite motility, defective ER architecture in *Pbyop1Δ* sporozoites could impact the efficiency of vesicle formation and/or transport. In turn, this would slow down sporozoite movement. A defect in ER structure may also affect the biogenesis of micronemes that contain adhesins secreted onto the parasite surface during sporozoite movement and affect turnover of adhesion sites.

The relatively modest effect of *PbYOP1*'s loss on sporozoite infectivity and development into liver stages may suggest that the ER in asexual stages and sporozoites is shaped by different tubule-forming protein(s), acting either alone or in concert with other homologs. There are differences in the predicted structures of *P. berghei*'s three putative ER tubule-forming proteins. The N-terminus of *PbYOP1* is much longer than those of *PbYOP1L* and *PbRTN1*. The first transmembrane helix of *PbYOP1L* and the second transmembrane helix of *PbRTN1* are shorter than the other transmembrane helix, suggesting they traverse the lipid bilayer only partially. The loop between the two transmembrane helices in *P. berghei* RTN1 (*PbRTN1*) is much longer than that of *PbYOP1* and *PbYOP1L* (Sun *et al.*, 2016). These differences suggest that individual reticulons could have distinct effects on membrane curvature *in vivo* and provide a strong rationale for investigation of their individual functions.

It is remarkable that the absence of a single intracellular protein, *PbYOP1* has a profound effect on the pathogenesis of ECM. ECM pathogenesis is complex and there are likely to be several mechanism(s) that underlie attenuation of ECM in *Pbyop1Δ*-infected mice. One possibility is that loss of ER architecture in these parasites impedes export of parasite proteins required for CD8⁺ T cell recruitment to the brain and their activation essential for ECM development (Baptista *et al.*, 2010; McQuillan *et al.*, 2011; Strangward *et al.*, 2017). Future work will investigate protein export to the RBC surface in *Pbyop1Δ* parasites.

ACKNOWLEDGMENTS

We thank Luke Fritzky of the NJMS Confocal Imaging Facility for technical assistance. This work was supported by NIH 5R01AI133633 and R21AI128052 to P.B., the National Key Research and Development Program (grant no. 2016YFA0500201) and the National Natural

Science Foundation of China (grant no. 31630020 and 91854202) to J.H., the open project by the National Laboratory of Macromolecules (2018kf05) and the startup funds from Tianjin Medical University (115004/000012 & 11601502/DW0114) to Q.W., and The Science & Technology Development Fund of Tianjin Education Commission for Higher Education (2016KJ0138 & 2018KJ085) to Q.W. and X.S.

DATA AVAILABILITY STATEMENT

Data that support the findings of this study are available from the corresponding author upon reasonable request.

ORCID

Purnima Bhanot  <https://orcid.org/0000-0001-5116-6973>

REFERENCES

- Abu Bakar, N., Klonis, N., Hanssen, E., Chan, C., and Tilley, L. (2010) Digestive-vacuole genesis and endocytic processes in the early intraerythrocytic stages of *Plasmodium falciparum*. *Journal of Cell Science*, *123*, 441–450.
- Agrawal, S.A., Burgoyne, T., Eblimit, A., Bellingham, J., Parfitt, D.A., Lane, A. *et al.* (2017) REEP6 deficiency leads to retinal degeneration through disruption of ER homeostasis and protein trafficking. *Human Molecular Genetics*, *26*, 2667–2677.
- Aikawa, M., Huff, C.G., and Spinz, H. (1966) Comparative feeding mechanisms of avian and primate malarial parasites. *Military Medicine*, *131*(Suppl. 9), 969–983.
- Allison, R., Edgar, J.R., Pearson, G., Rizo, T., Newton, T., Gunther, S. *et al.* (2017) Defects in ER-endosome contacts impact lysosome function in hereditary spastic paraplegia. *The Journal of Cell Biology*, *216*, 1337–1355.
- Anderson, D.J., and Hetzer, M.W. (2008) Reshaping of the endoplasmic reticulum limits the rate for nuclear envelope formation. *Journal of Cell Biology*, *182*, 911–924.
- Bannister, L.H., Hopkins, J.M., Fowler, R.E., Krishna, S., and Mitchell, G.H. (2000) A brief illustrated guide to the ultrastructure of *Plasmodium falciparum* asexual blood stages. *Parasitology Today*, *16*, 427–433.
- Baptista, F.G., Pamplona, A., Pena, A.C., Mota, M.M., Pied, S., and Vigario, A.M. (2010) Accumulation of *Plasmodium berghei*-infected red blood cells in the brain is crucial for the development of cerebral malaria in mice. *Infection and Immunity*, *78*, 4033–4039.
- Baumann, O., and Walz, B. (2001) Endoplasmic reticulum of animal cells and its organization into structural and functional domains. *International Review of Cytology*, *205*, 149–214.
- Blackstone, C., O'Kane, C.J., and Reid, E. (2011) Hereditary spastic paraplegias: membrane traffic and the motor pathway. *Nature Reviews Neuroscience*, *12*, 31–42.
- Brady, J.P., Claridge, J.K., Smith, P.G., and Schnell, J.R. (2015) A conserved amphipathic helix is required for membrane tubule formation by Yop1p. *Proceedings of the National Academy of Sciences of the United States of America*, *112*, E639–648.
- Breuss, M.W., Nguyen, A., Song, Q., Nguyen, T., Stanley, V., James, K.N. *et al.* (2018) Mutations in LNPk, encoding the endoplasmic reticulum junction stabilizer lunapark, cause a recessive neurodevelopmental syndrome. *American Journal of Human Genetics*, *103*, 296–304.
- Burda, P.C., Schaffner, M., Kaiser, G., Roques, M., Zuber, B., and Heussler, V.T. (2017) A *Plasmodium* plasma membrane reporter reveals membrane dynamics by live-cell microscopy. *Scientific Reports*, *7*, 1–4.
- Bushell, E., Gomes, A.R., Sanderson, T., Anar, B., Girling, G., Herd, C. *et al.* (2017) Functional profiling of a *Plasmodium* genome reveals an abundance of essential genes. *Cell*, *170*(2), 260–272.e8.
- Chen, J., Stefano, G., Brandizzi, F., and Zheng, H. (2011) Arabidopsis RHD3 mediates the generation of the tubular ER network and is required for Golgi distribution and motility in plant cells. *Journal of Cell Science*, *124*, 2241–2252.
- Chen, S., Desai, T., McNew, J.A., Gerard, P., Novick, P.J., and Ferro-Novick, S. (2015) Lunapark stabilizes nascent three-way junctions in the endoplasmic reticulum. *Proceedings of the National Academy of Sciences of the United States of America*, *112*, 418–423.
- Chen, S., Novick, P., and Ferro-Novick, S. (2012) ER network formation requires a balance of the dynamin-like GTPase Sey1p and the Lunapark family member Lnp1p. *Nature Cell Biology*, *14*, 707–716.
- Dluzewski, A.R., Ling, I.T., Hopkins, J.M., Grainger, M., Margos, G., Mitchell, G.H. *et al.* (2008) Formation of the food vacuole in *Plasmodium falciparum*: a potential role for the 19 kDa fragment of merozoite surface protein 1 (MSP1(19)). *PLoS One*, *3*, e3085.
- Francis, S.E., Sullivan, D.J. Jr, and Goldberg, D.E. (1997) Hemoglobin metabolism in the malaria parasite *Plasmodium falciparum*. *Annual Review of Microbiology*, *51*, 97–123.
- Frohlich, F., Petit, C., Kory, N., Christiano, R., Hannibal-Bach, H.K., Graham, M. *et al.* (2015) The GARP complex is required for cellular sphingolipid homeostasis. *Elife*, *4*, e08712.
- Galway, M.E., Heckman, J.W. Jr, and Schiefelbein, J.W. (1997) Growth and ultrastructure of Arabidopsis root hairs: the rhd3 mutation alters vacuole enlargement and tip growth. *Planta*, *201*, 209–218.
- Goldberg, D.E. (1993) Hemoglobin degradation in *Plasmodium*-infected red blood cells. *Seminars in Cell Biology*, *4*, 355–361.
- Gras, S., Jimenez-Ruiz, E., Klinger, C.M., Schneider, K., Klingl, A., Lemgruber, L. *et al.* (2019) An endocytic-secretory cycle participates in *Toxoplasma gondii* motility. *PLoS Biology*, *17*, e3000060.
- Hanssen, E., Sougrat, R., Frankland, S., Deed, S., Klonis, N., Lippincott-Schwartz, J. *et al.* (2008) Electron tomography of the Maurer's cleft organelles of *Plasmodium falciparum*-infected erythrocytes reveals novel structural features. *Molecular Microbiology*, *67*, 703–718.
- Hegge, S., Kudryashev, M., Smith, A., and Frischknecht, F. (2009) Automated classification of *Plasmodium* sporozoite movement patterns reveals a shift towards productive motility during salivary gland infection. *Biotechnology Journal*, *4*, 903–913.
- Hegge, S., Munter, S., Steinbuchel, M., Heiss, K., Engel, U., Matuschewski, K. *et al.* (2010) Multistep adhesion of *Plasmodium* sporozoites. *FASEB Journal*, *24*, 2222–2234.
- Hu, J., Prinz, W.A., and Rapoport, T.A. (2011) Weaving the web of ER tubules. *Cell*, *147*, 1226–1231.
- Hu, J., Shibata, Y., Zhu, P.P., Voss, C., Rismanchi, N., Prinz, W.A. *et al.* (2009) A class of dynamin-like GTPases involved in the generation of the tubular ER network. *Cell*, *138*, 549–561.
- Hu, Y., Zhong, R., Morrison, W.H. 3rd, and Ye, Z.H. (2003) The Arabidopsis RHD3 gene is required for cell wall biosynthesis and actin organization. *Planta*, *217*, 912–921.
- Ingmundson, A., Alano, P., Matuschewski, K., and Silvestrini, F. (2014) Feeling at home from arrival to departure: protein export and host cell remodelling during *Plasmodium* liver stage and gametocyte maturation. *Cellular Microbiology*, *16*, 324–333.
- Janse, C.J., Haghighparast, A., Speranca, M.A., Ramesar, J., Kroeze, H., del Portillo, H.A. *et al.* (2003) Malaria parasites lacking eef1a have a normal S/M phase yet grow more slowly due to a longer G1 phase. *Molecular Microbiology*, *50*, 1539–1551.
- Janse, C.J., Ramesar, J., and Waters, A.P. (2006) High-efficiency transfection and drug selection of genetically transformed blood stages of the rodent malaria parasite *Plasmodium berghei*. *Nature Protocols*, *1*, 346–356.
- Kaiser, G., De Niz, M., Zuber, B., Burda, P.C., Kornmann, B., Heussler, V.T. *et al.* (2016) High resolution microscopy reveals an unusual architecture of the *Plasmodium berghei* endoplasmic reticulum. *Molecular Microbiology*, *102*, 775–791.

- Kennedy, M., Fishbaugher, M.E., Vaughan, A.M., Patrapuvich, R., Boonhok, R., Yimamnuaychok, N. *et al.* (2012) A rapid and scalable density gradient purification method for *Plasmodium* sporozoites. *Malaria Journal*, *11*, 421.
- Klemba, M., Beatty, W., Gluzman, I., and Goldberg, D.E. (2004) Trafficking of plasmepsin II to the food vacuole of the malaria parasite *Plasmodium falciparum*. *The Journal of Cell Biology*, *164*, 47–56.
- Lai, Y.S., Stefano, G., and Brandizzi, F. (2014) ER stress signaling requires RHD3, a functionally conserved ER-shaping GTPase. *Journal of Cell Science*, *127*, 3227–3232.
- Lazarus, M.D., Schneider, T.G., and Taraschi, T.F. (2008) A new model for hemoglobin ingestion and transport by the human malaria parasite *Plasmodium falciparum*. *Journal of Cell Science*, *121*, 1937–1949.
- Lee, S.H., Hadipour-Lakmehsari, S., Murthy, H.R., Gibb, N., Miyake, T., Teng, A.C.T. *et al.* (2020) REEP5 depletion causes sarco-endoplasmic reticulum vacuolization and cardiac functional defects. *Nature Communications*, *11*, 1–20.
- McQuillan, J.A., Mitchell, A.J., Ho, Y.F., Combes, V., Ball, H.J., Golenser, J. *et al.* (2011) Coincident parasite and CD8 T cell sequestration is required for development of experimental cerebral malaria. *International Journal for Parasitology*, *41*, 155–163.
- Nishi, M., Hu, K., Murray, J.M., and Roos, D.S. (2008) Organellar dynamics during the cell cycle of *Toxoplasma gondii*. *Journal of Cell Science*, *121*, 1559–1568.
- Niu, L., Ma, T., Yang, F., Yan, B., Tang, X., Yin, H. *et al.* (2019) Atlastin-mediated membrane tethering is critical for cargo mobility and exit from the endoplasmic reticulum. *Proceedings of the National Academy of Sciences of the United States of America*, *116*, 14029–14038.
- Opperdoes, F.R., Baudhuin, P., Coppens, I., De Roe, C., Edwards, S.W., Weijers, P.J. *et al.* (1984) Purification, morphometric analysis, and characterization of the glycosomes (microbodies) of the protozoan hemoflagellate *Trypanosoma brucei*. *The Journal of Cell Biology*, *98*, 1178–1184.
- World Health Organization (2019) World malaria report 2019, Geneva. Licence: CC BY-NC-SA 3.0 IGO.
- Orso, G., Pendin, D., Liu, S., Toso, J., Moss, T.J., Faust, J.E. *et al.* (2009) Homotypic fusion of ER membranes requires the dynamin-like GTPase atlastin. *Nature*, *460*, 978–983.
- Pisciotta, J.M., Scholl, P.F., Shuman, J.L., Shulev, V., and Sullivan, D.J. (2017) Quantitative characterization of hemozoin in *Plasmodium berghei* and *vivax*. *International Journal for Parasitology: Drugs and Drug Resistance*, *7*, 110–119.
- Shemesh, T., Klemm, R.W., Romano, F.B., Wang, S., Vaughan, J., Zhuang, X. *et al.* (2014) A model for the generation and interconversion of ER morphologies. *Proceedings of the National Academy of Sciences of the United States of America*, *111*, E5243–E5251.
- Shibata, Y., Voeltz, G.K., and Rapoport, T.A. (2006) Rough sheets and smooth tubules. *Cell*, *126*, 435–439.
- Sinnis, P., De La Vega, P., Coppi, A., Krzych, U., & Mota, M.M. (2013) Quantification of sporozoite invasion, migration, and development by microscopy and flow cytometry. *Methods in Molecular Biology*, *923*, 385–400.
- Spaccapelo, R., Janse, C.J., Caterbi, S., Franke-Fayard, B., Bonilla, J.A., Syphard, L.M. *et al.* (2010) Plasmeprin 4-deficient *Plasmodium berghei* are virulence attenuated and induce protective immunity against experimental malaria. *American Journal of Pathology*, *176*, 205–217.
- Spielmann, T., and Gilberger, T.W. (2015) Critical steps in protein export of *Plasmodium falciparum* blood stages. *Trends in Parasitology*, *31*, 514–525.
- Storm, J., and Craig, A.G. (2014) Pathogenesis of cerebral malaria—Inflammation and cytoadherence. *Frontiers in Cellular and Infection Microbiology*, *4*, 100.
- Strangward, P., Haley, M.J., Shaw, T.N., Schwartz, J.M., Greig, R., Mironov, A. *et al.* (2017) A quantitative brain map of experimental cerebral malaria pathology. *PLoS Pathogens*, *13*, e1006267.
- Sun, S., Lv, L., Yao, Z., Bhanot, P., Hu, J., and Wang, Q. (2016) Identification of endoplasmic reticulum-shaping proteins in *Plasmodium* parasites. *Protein Cell*, *7*, 615–620.
- Teixeira, J.E., and Huston, C.D. (2008) Evidence of a continuous endoplasmic reticulum in the protozoan parasite *Entamoeba histolytica*. *Eukaryotic Cell*, *7*, 1222–1226.
- van Dooren, G.G., Marti, M., Tonkin, C.J., Stimmler, L.M., Cowman, A.F., and McFadden, G.I. (2005) Development of the endoplasmic reticulum, mitochondrion and apicoplast during the asexual life cycle of *Plasmodium falciparum*. *Molecular Microbiology*, *57*, 405–419.
- Veleri, S., Nellissery, J., Mishra, B., Manjunath, S.H., Brooks, M.J., Dong, L. *et al.* (2017) REEP6 mediates trafficking of a subset of Clathrin-coated vesicles and is critical for rod photoreceptor function and survival. *Human Molecular Genetics*, *26*, 2218–2230.
- Villegas-Mendez, A., Greig, R., Shaw, T.N., de Souza, J.B., Gwyer Findlay, E., Stumhofer, J.S. *et al.* (2012) IFN-gamma-producing CD4+ T cells promote experimental cerebral malaria by modulating CD8+ T cell accumulation within the brain. *The Journal of Immunology*, *189*, 968–979.
- Voeltz, G.K., Prinz, W.A., Shibata, Y., Rist, J.M., and Rapoport, T.A. (2006) A class of membrane proteins shaping the tubular endoplasmic reticulum. *Cell*, *124*, 573–586.
- Wang, H., Lockwood, S.K., Hoeltzel, M.F., and Schiefelbein, J.W. (1997) The ROOT HAIR DEFECTIVE3 gene encodes an evolutionarily conserved protein with GTP-binding motifs and is required for regulated cell enlargement in *Arabidopsis*. *Genes & Development*, *11*, 799–811.
- Wang, S., Powers, R.E., Gold, V.A., and Rapoport, T.A. (2018) The ER morphology-regulating lunapark protein induces the formation of stacked bilayer discs. *Life Science Alliance*, *1*, e201700014.
- Wang, S., Tukachinsky, H., Romano, F.B., and Rapoport, T.A. (2016) Cooperation of the ER-shaping proteins atlastin, lunapark, and reticulons to generate a tubular membrane network. *eLife*, *5*, e18605.
- Wang, X., Li, S., Wang, H., Shui, W., and Hu, J. (2017) Quantitative proteomics reveal proteins enriched in tubular endoplasmic reticulum of *Saccharomyces cerevisiae*. *Elife*, *6*, e23816.
- Westrate, L.M., Lee, J.E., Prinz, W.A., and Voeltz, G.K. (2015) Form follows function: the importance of endoplasmic reticulum shape. *Annual Review of Biochemistry*, *84*, 791–811.
- Wu, H., Carvalho, P., and Voeltz, G.K. (2018) Here, there, and everywhere: The importance of ER membrane contact sites. *Science*, *361*, eaan5835.
- Yalcin, B., Zhao, L., Stofanko, M., O'Sullivan, N.C., Kang, Z.H., Roost, A. *et al.* (2017) Modeling of axonal endoplasmic reticulum network by spastic paraplegia proteins. *Elife*, *6*, e23882.
- Yao, L., Xie, D., Geng, L., Shi, D., Huang, J., Wu, Y. *et al.* (2018) REEP5 (Receptor Accessory Protein 5) acts as a sarcoplasmic reticulum membrane sculptor to modulate cardiac function. *Journal of the American Heart Association*, *7*(3), e007205.
- Zhou, X., He, Y., Huang, X., Guo, Y., Li, D., and Hu, J. (2019) Reciprocal regulation between lunapark and atlastin facilitates ER three-way junction formation. *Protein & Cell*, *10*, 510–525.

SUPPORTING INFORMATION

Additional Supporting Information may be found online in the Supporting Information section.

How to cite this article: Shi X, Hai L, Govindasamy K, et al. A *Plasmodium* homolog of ER tubule-forming proteins is required for parasite virulence. *Mol Microbiol*. 2020;114: 454–467. <https://doi.org/10.1111/mmi.14526>